A fast self-tuning method for PID parameters of AMBs based on Deep Deterministic Policy Gradient algorithm

Qiqi JIANG*, Jin ZHOU*, Yuanping XU*, Chaowu JIN*, and Yue ZHANG*
*College of Mechanical & Electrical Engineering, Nanjing University of Aeronautics and Astronautics
Qinhuai, Nanjing, Jingsu 210016, China
E-mail: qqj77@nuaa.edu.cn

Abstract
Active magnetic bearing(AMB) is an advanced contactless bearing system for high rotation speed equipment but cannot work stably without closed-loop control. Normally multiple proportional integral derivative (PID) controllers are used to control the multi-axis AMB system. However, existing AMB PID controller tuning methods mainly focus on optimization and cannot turn an AMB system from unstable to stable. In this article, a model free AMB PID self-tuning method based on the Deep Deterministic Policy Gradient (DDPG) algorithm is proposed to solve this problem. This approach enables the autonomous tuning of PID controller parameters via the DDPG algorithm. Additionally, a rapidly convergent reward function design method applicable to large action spaces is introduced to enhance the proposed algorithm's general applicability and validated. For an unknown and untuned AMB system, the proposed tuning method provides a viable parameter solution within a short timeframe while delivering acceptable performance. Furthermore, the designed DDPG-based self-tuner demonstrates acceptable robust capabilities under sinusoidal, step, impulse, and composite disturbances. The proposed self-tuning method not only reduces controller design complexity but also provides a foundation for the engineering application of AMB system.

Keywords : Active magnetic bearing, PID controller, DDPG, Parameter self-tuning, Composite disturbance.

1. Introduction

Active Magnetic Bearing (AMB) utilize controllable electromagnetic forces for contactless rotor levitation, offering frictionless operation, no lubrication requirement, low power consumption, and high-speed capability. it provides a revolutionary solution for high-speed rotating machinery, now widely implemented in high-power blowers, compressors, vacuum pumps, and refrigeration systems, significantly reducing energy consumption (Koehler et al., 2017).

However, AMB systems are inherently open-loop unstable and require closed-loop control for stable operation. PID controllers (and their variants) are widely used in industry due to their simple structure and clear physical interpretation, remaining the dominant control strategy for AMBs. PID performance relies heavily on parameters (proportional gain k_P, integral gain k_I, derivative gain k_D). Unfortunately, AMBs exhibit strong nonlinearity, multi-DOF coupling, and time-varying disturbances (e.g., imbalance vibration (Yu et al., 2025), load variations from air pressure/flow changes (Li et al., 2025), and random impacts from valve actuation (Zhang et al., 2025)), making manual tuning tedious, time-consuming, and expert-dependent. Critically, improper tuning can lead to system oscillation, slow response, or even instability. To address these tuning challenges, various methods have been proposed, including:

(1) Methods based on experience, such as trial-and-error and Ziegler-Nichols techniques: The former manually adjusts parameters based on real-time system responses (overshoot, steady-state error, etc.) until requirements are met. The latter calculates PID parameters using empirical formulas (Sarmah and Tiwari, 2022). Although conceptually simple, these methods exhibit poor robustness, require significant time investment, and depend heavily on expert experience.

(2) Methods based on Model, such as pole placement and Linear Quadratic Regulator, derive PID parameters through mathematical modeling of rotor dynamics (Hutterer et al., 2020), typically requiring preliminary system identification. While effective for AMBs with simple rotor structures under consistent operating conditions, these methods face limitations in industrial applications due to time-varying disturbances. Crucially, accurate system identification prior to PID parameter tuning is often unattainable in practical AMB implementations.

(3) Methods based on heuristic algorithms, such as Particle Swarm Optimization and fuzzy PID controllers: The

former conduct offline searches for parameters (Laldingliana and Biswas, 2022), yet incurs high computational overhead and lacks online adaptive capability. Separately, fuzzy PID enables online adaptive tuning, making it suitable for AMB systems operating under disturbance conditions (Liu et al., 2022). However, this approach is ineffective for systems requiring continuous large-range parameter adjustments and exhibits chattering during abrupt operational transitions.

Despite the advantages of the parameter tuning methods mentioned above, designing an experience-free, model-agnostic approach capable of generating continuous control actions to stabilize initially unstable AMB rotors remains a significant challenge. The Deep Deterministic Policy Gradient (DDPG), a model-free reinforcement learning algorithm, excels in continuous control domains (Mousavifard et al., 2025) and offers model-free learning, continuous PID parameter generation, online adaptation without expert intervention. These characteristics make DDPG highly promising for self-tuning controller parameters in complex systems like AMBs, though current research remains limited. However, significant challenges persist in direct DDPG application to AMB PID tuning:①Unstable AMB operation risks rotor touchdown;②Requires simultaneously ensuring algorithm convergence and robust dynamic performance under time-varying disturbances;③Demands flexible search ranges for diverse AMBs.

Addressing these challenges, this work aims to resolve technical obstacles in applying DDPG for PID parameter self-tuning in AMBs, ultimately achieving safe self-tuning, efficient and robust. The primary innovations include:

(1) A DDPG-Based PID self-tuning framework is proposed to simplifying the tuning process for AMBs, eliminating manual intervention.

(2) A safety-embedded reward function is designed during DDPG exploration to prevent rotor touchdown.

(3) A generalized action-space DDPG algorithm is improved to enable wide-span parameter searches with accelerated convergence for diverse AMB configurations, ensuring broad applicability.

This article is organized as follows. The AMBs modeling is given in Section II. Then, the DDPG fundamental and improved self-tuning method are presented in Section III. Based on the proposed DDPG algorithm, a multi-disturbance rejection scheme for comprehensive validation is conducted in Section IV. Finally, Section V concludes the work.

2. Modeling of AMBs

Considering no additional factors such as rotor flexible deformation are involved and the fact that the axial and radial motion can be decoupled, a 4-DOF rigid rotor is finally selected as the research object. The content of this section is divided into two parts: (1) Modeling of a 4-DOF maglev rotor; (2) Modeling of a 4-DOF closed-loop AMBs.

2.1 AMB-rotor system

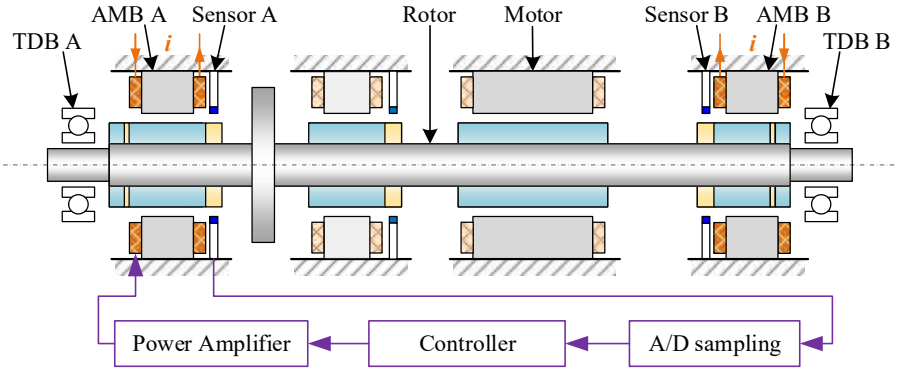

(a) Structure diagram of AMBs

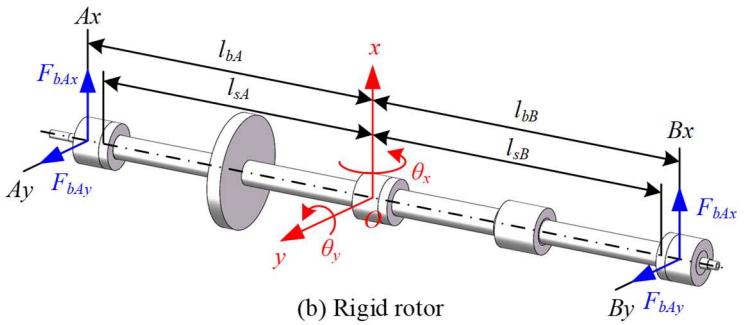

(b) Rigid rotor

Fig. 1 Structure of the AMB-supported system

The studied rigid rotor system supported by AMB is illustrated in Fig. 1. As shown in Fig. 1(a), the whole system contains an imbalance rotor, a pair of radial AMB, a pair of touch-down bearing, displacement sensors, power amplifiers, a digital controller, and a PMSM. The rotor is supported by the radial AMB, and the TDBs are merely for power-off protection. The PMSM between the two AMB is driven by a variable-frequency converter whose purpose is to control the rotational speed. A Cartesian coordinate system is established at the rotor centroid in Fig. 1(b). Using the generalized coordinates $\boldsymbol{q_c} = [x_c, \theta_x, y_c, \theta_y]$, the rotor dynamics model derived from Lagrange's theorem can be obtained as

$$\boldsymbol{M}\ddot{\boldsymbol{q}}_c + \boldsymbol{G}\dot{\boldsymbol{q}}_c = \boldsymbol{F}_{unb} + \boldsymbol{T}_b\boldsymbol{F}_b + \boldsymbol{T}_g\boldsymbol{F}_g + \boldsymbol{T}_d F_d \tag{1}$$

Where $\boldsymbol{F_g}$, $\boldsymbol{F_b}$, $\boldsymbol{F_{unb}}$, and $\boldsymbol{F_d}$ denote the gravity of the rotor, AMB force, centrifugal force caused by rotor unbalance and external disturbance force, respectively. The expressions of $\boldsymbol{M}$, $\boldsymbol{G}$, and $\boldsymbol{F_{unb}}$ are given by:

$$\boldsymbol{M} = \begin{bmatrix} m & 0 & 0 & 0 \\ 0 & J_r & 0 & 0 \\ 0 & 0 & m & 0 \\ 0 & 0 & 0 & J_r \end{bmatrix}, \boldsymbol{G} = \dot{\theta}_z \begin{bmatrix} 0 & 0 & 0 & 0 \\ 0 & 0 & 0 & J_z \\ 0 & 0 & 0 & 0 \\ 0 & -J_z & 0 & 0 \end{bmatrix}$$

$$\boldsymbol{F}_{unb} = \dot{\theta}_z^{\,2} \begin{bmatrix} me\cos(\theta_z + \theta_{unb1}) \\ -J_r\sigma\sin(\theta_z + \theta_{unb2}) \\ me\sin(\theta_z + \theta_{unb1}) \\ J_r\sigma\cos(\theta_z + \theta_{unb2}) \end{bmatrix} + \ddot{\theta}_z \begin{bmatrix} me\sin(\theta_z + \theta_{unb1}) \\ J_r\sigma\cos(\theta_z + \theta_{unb2}) \\ -me\cos(\theta_z + \theta_{unb1}) \\ J_r\sigma\sin(\theta_z + \theta_{unb2}) \end{bmatrix}, \boldsymbol{T_b} = \begin{bmatrix} 1 & 0 & 1 & 0 \\ 0 & l_{bA} & 0 & -l_{bB} \\ 0 & 1 & 0 & 1 \\ -l_{bA} & 0 & l_{bB} & 0 \end{bmatrix}$$

Where m represents the rotor mass and $\dot{\theta}_z$ denotes the rotational speed. Given $\dot{\theta}_z = 0$, the centrifugal force induced by mass imbalance can be negligible. The AMB force $\boldsymbol{F_b} = [\boldsymbol{F_{bAx}}, \boldsymbol{F_{bAy}}, \boldsymbol{F_{bBx}}, \boldsymbol{F_{bBy}}]$ is linear in operating range. As a result, a linear model is analyzed instead as follows:

$$F_{bAx} = k_x x_{Ax}(t) + k_i\left(i_{Ax}(t) + i_{gAx}\right) = k_x x_{Ax}(t) + k_i i_{Ax}(t) + k_i i_{gAx} = k_x x(t) + k_i i(t) + F_{gAx} \tag{2}$$

Where $(i_{Ax}(t)+i_{gAx})$ denotes the control current, k_i represents the force/current stiffness, k_x represents the force/displacement stiffness, and x_{Ax} represents the rotor displacement at the AMB. Due to the rotor mass being constant, a constant gravity compensation control current i_{gAx} can compensate the gravity F_{gAx} of the rotor. Thus, $k_i i_{gAx} = F_{gAx} = mg_{Ax}$, and $i_{Ax}(t)$ represents the motion control current which influences the motion of the controlled rotor in real.

Since rotor displacement is experimentally measurable, the generalized coordinates are defined as $\boldsymbol{q_s} = [Ax, Ay, Bx, By]$. The rotor dynamics model in this coordinate system then yields:

$$\boldsymbol{M}\left(\boldsymbol{T}_s\ddot{\boldsymbol{q}}_s\right) + \boldsymbol{G}\left(\boldsymbol{T}_s\dot{\boldsymbol{q}}_s\right) = \boldsymbol{F}_{unb} + \boldsymbol{T}_b\left(\boldsymbol{k}_x\boldsymbol{T}_a^{-1}\boldsymbol{T}_s\boldsymbol{q}_s + \boldsymbol{k}_i\boldsymbol{i}\right) + \boldsymbol{T}_d\boldsymbol{F}_d \tag{3}$$

Where $\boldsymbol{T_s}$ denotes the transformation matrix between generalized coordinates $\boldsymbol{q_s}$ and $\boldsymbol{q_c}$, and $\boldsymbol{T_a}$ represents the displacement transformation matrix from the AMB location to sensor locations.

$$\boldsymbol{T}_s = \frac{1}{l_{sA}+l_{sB}} \begin{bmatrix} l_{sB} & 0 & l_{sA} & 0 \\ 0 & 1 & 0 & -1 \\ 0 & l_{sB} & 0 & l_{sA} \\ 1 & 0 & 1 & 0 \end{bmatrix}, \quad \boldsymbol{T}_a = \frac{1}{l_{bA}+l_{bB}} \begin{bmatrix} l_{bB} & 0 & l_{bA} & 0 \\ 0 & 1 & 0 & -1 \\ 0 & l_{bB} & 0 & l_{bA} \\ 1 & 0 & 1 & 0 \end{bmatrix}$$

2.2 Closed-loop system

To ensure AMBs stability, a closed-loop control including displacement sensors, PID controller, and power amplifier must be implemented. The displacement sensor exhibits an effective measurement bandwidth of 5 kHz, significantly higher than the operating speed. Thus, its transfer function $G_s(s)$ can be considered as an ideal proportional gain:

$$G_s(s) = k_s = 20000\left(\mathrm{V}/\mu\mathrm{m}\right) \tag{4}$$

The transfer function of PID controller and three-level PWM switching amplifier can be expressed as:

$$G_c(s) = k_P + k_I\frac{1}{s} + k_D\frac{s}{\tau s + 1} \tag{5}$$

$$G_a(s) = k_a \frac{1}{\tau_a s + 1} \frac{1}{\tau_b s + 1} \tag{6}$$

Where k_P, k_I, k_D denote PID controller parameters, τ represents the time constant of the incomplete derivative term, k_a denotes the amplifier gain, with $\tau_a = 1/(2\pi\times2000)$ and $\tau_b = 1/(2\pi\times3000)$. Combined with the rigid rotor model, the closed-loop system block diagram is shown in Fig. 2. The transfer function of control current can be expressed as:

$$I(s) = Q(s) G_a(s) G_c(s) G_s(s) \tag{7}$$

Substituting into Eq. (3) yields the Laplace-transformed system dynamics equation:

$$\boldsymbol{M}\boldsymbol{T}_s s^2 Q(s) + \boldsymbol{G}\boldsymbol{T}_s s Q(s) - \left[\boldsymbol{T}_b \boldsymbol{k}_x \boldsymbol{T}_a^{-1} \boldsymbol{T}_s + \boldsymbol{T}_b \boldsymbol{k}_i \frac{k_a}{T_a s + 1} \frac{k_s}{T_b s + 1} \left(k_P + k_I \frac{1}{s} + k_D \frac{s}{\tau s + 1} \right) \right] Q(s) = \boldsymbol{T}_d \boldsymbol{F}_d \tag{8}$$

Normally, the conventional PID controller parameters can be derived using Equation 8.

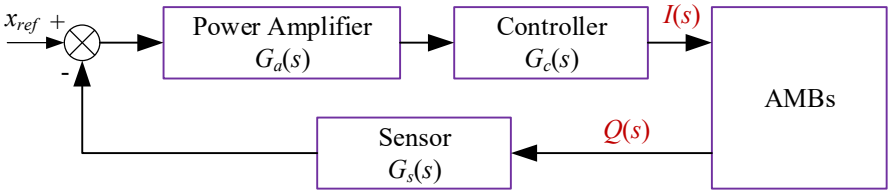

Fig. 2 Block diagram of the closed-loop system

3. Design of Deep Deterministic Policy Gradient algorithm

This subsection presents the DDPG-based controller self-tuning methodology, covering three key aspects:(1) DDPG algorithm fundamentals; (2) Design of reward function; (3) Training of AMB-DDPG

3.1 The operating rule of DDPG

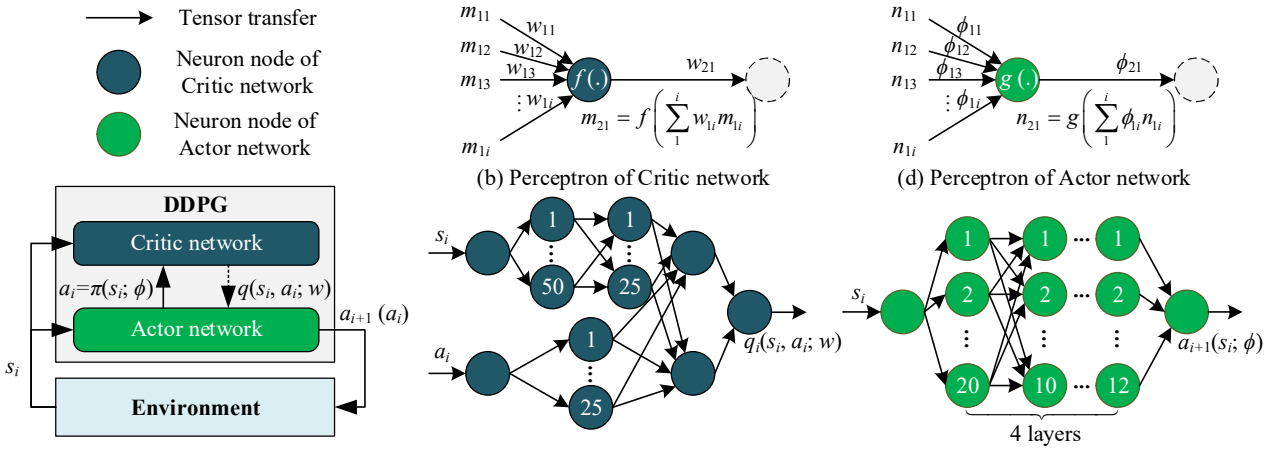

(a) The principle of DDPG (b) Perceptron of Critic network (c) Structure of Critic network (d) Perceptron of Actor network (e) Structure of Actor network

Fig. 3 The principle of DDPG and the structure of actor network and critic network

DDPG, which relies on the Actor-Critic framework, handles continuous action spaces. Its working mechanism is depicted in Fig. 3(a). The algorithm uses the Actor network to estimate the policy π and the Critic network to approximate the value function q, enabling end-to-end learning. Both the Actor and Critic networks incorporate a training network and a target network. The architectural designs of the Actor and Critic networks for DDPG are presented in Fig. 3(b) and Fig. 3(c), respectively. The Actor network takes the agent's motion states as input and generates an action a that maximizes the value function $q(s, a)$ for the given state s, thereby implementing a deterministic policy $a = \pi(s)$.

$$\pi(s) = \arg\max q(s, a) \tag{9}$$

The Critic network receives the agent's movement state s and the action a from the Actor network, and outputs the estimated value q. The Critic network typically employs the mean square Bellman error (MSBE) to assess the discrepancy between the neural network's estimated value q and the target derived from the Bellman equation, that is

$$L = E\left[r_i + \gamma q'\left(s_{i+1}, \pi'\left(s_{i+1}|\phi'\right)|w'\right) - q\left(s_i, a_i|w\right)\right]^2 \tag{10}$$

Where q' represents q value at time t+1, and ϕ', w' w represents the variables in the Actor target network, Critic target network, and Critic network respectively. γ expresses the discount factor of Bellman equation. The gradient update rule of the Actor network is

$$\nabla_\phi J \approx E\left[\nabla_a q\left(s, a|w\right)\Big|_{s=s_i, a=\pi(s_i)} \nabla_\phi \pi\left(s|\phi\right)|s_i\right] \tag{11}$$

Where ϕ represents the variables in the Critic target network. Both the Actor and Critic target networks employ the soft update approach for network parameter updates. The parameter update rules are as follows.

$$\begin{aligned} w' &\leftarrow \tau \bullet w + (1-\tau) w' \\ \phi' &\leftarrow \tau \bullet \phi + (1-\tau) \phi' \end{aligned} \tag{12}$$

Where τ denotes the hyper parameter of softness and hardness.

1. Randomly initialize DDPG network $q(s, a; w)$, and $\pi(s; \phi)$ with random parameter w, ϕ;
2. Initialize target network q' and π' with weights $w' \leftarrow w$, $\phi' \leftarrow \phi$;
3. Initialize Replay Buffer B;
4. **For** episode = 1, M **do**:
   - Initialize a random process ξ for action exploration;
   - Receive initial observation state s_1;
   - **For** t = 1, T **do**
     - Select action with exploration $a_t \sim \pi(s; \phi)+\varepsilon$, $\varepsilon \sim \xi(0, \sigma)$;
     - Execute action a_t and observe reward r_t and new state s_{t+1};
     - Store transition (s_t, a_t, r_t, s_{t+1}) in B;
     - Sample a random minibatch of N transition (s_i, a_i, r_i, s_{i+1}) in B;
     - Set $y_i = r_i + \gamma q'\left(s_{i+1}, \pi'\left(s_{i+1}|\phi'\right)|w'\right)$;
     - Update critic by minimizing the loss L according to Eq. (10)
     - Update the actor network using the sampled policy gradient according to Eq. (11)
     - Set a hyper-parameter $\tau \in (0,1)$;
     - Update the target networks according to Eq. (12)
   - **End for**
4. **End for**

3.2 Design of reward function

The DDPG algorithm's learning objective is to discover control policies that stabilize the rotor at its equilibrium point. Drawing upon PD control principles, the reward function is designed as follows:

$$\begin{aligned} r &= r_{dis\_P} + r_{vel\_c} + r_{dis\_O} + r_{dis\_e} + r_{exceed} = a_1 \frac{|e_{\max}| - |e|}{e + e_0} + a_2 \frac{|v_{\max}| - |v|}{|v_{\max}|} + a_3 \left(\left| \frac{e}{|e|} - \frac{v}{|v|} \right| - 1 \right) + f(e) + g(e, v) \\ f(e) &= \begin{cases} a_4, & e \in 0.1(e_{\min}, e_{\max}) \\ \cdots & \\ a_i, & e \in (e_{\min}, e_{\max}) \end{cases}, g(e) = \begin{cases} a_{i+1}, & e \notin (e_{\min}, e_{\max}) \\ a_{i+2}, & v \notin (v_{\min}, v_{\max}) \end{cases} \end{aligned} \tag{12}$$

Where a_1, a_2, …, a_{i+2} are weighting coefficients. The displacement proportional term r_{dis_P} is defined such that reward increases as the rotor approaches its equilibrium point and decreases with deviation, which directly minimizes position error. The velocity damping term r_{vel_c} is designed to scale reward proportionally with absolute rotor speed magnitude, which introduces virtual damping to enhance system stability.

To accelerate DDPG convergence, a motion guidance term $r_{dis\_O} + r_{dis\_e}$ is designed. Specially, r_{dis_O} rewards motion toward equilibrium and penalizes deviation. r_{dis_e} proportionally rewards proximity to equilibrium but operates directly on error magnitude, synergistically enhancing convergence. Expanding the search space to meet the requirements of diverse AMBs is need for DDPG algorithm. However, large-range searching significantly reduces convergence speed and certain parameters may fail to ensure stable levitation in offline simulation. To mitigate these issues, a threshold term r_{exceed} is designed to penalize when the rotor displacement exceeds the TDB clearance.

3.3 Training of AMB-DDPG

The block diagram for DDPG-based PID controller self-tuning in AMB is shown in Fig. 4. The actor network is designed to autonomously output PID parameter values, while the critic network evaluates these parameters based on reward functions, and feeds back the evaluation value to the actor network, enabling the actor network to generate PID parameter with higher evaluation values. Relevant parameters of rotor and network are detailed in Table. 1.

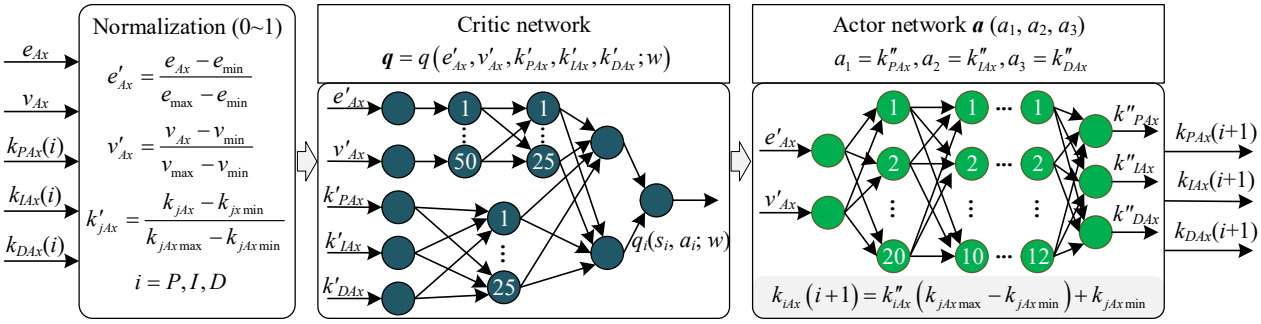

Fig. 4 Training block diagram for parameter self-tuning of PID controller for AMB based on DDPG

4. Performance of PID controller with DDPG algorithm

This section analyzes the performance and effectiveness of DDPG-based PID for AMB under typical engineering disturbances. The content is divided into: (1) Analysis of initiation levitation; (2) Response to sinusoidal disturbance; (3) Response to step disturbance; (4) Response to impulse disturbance; (5) Response to composite disturbance.

4.1 Results of initial levitation

To validate the DDPG controller, a comparative study on initiation levitation is designed. A single degree of freedom *Ax* is controlled by DDPG-tuned PID, while the remaining three DOFs (*Ay*, *Bx*, *By*) employ conventional PID with parameters selected by natural/damping stiffness principles $k_P = 2k_x/k_i/k_a/k_s$ and $k_D = 2\xi\sqrt{mk_x}/k_i/k_a/k_s$. The parameters are shown in Table. 1.

Table 1 PID parameters in the direction of *Ax*、*Ay*、*Bx*、*By*

	k_P	k_I	K_D
Ax	0.1~10	0.1~10	0.001~0.01
Ay	1.8	1	0.0014
Bx	1.8	1	0.0014
By	1.8	1	0.0014

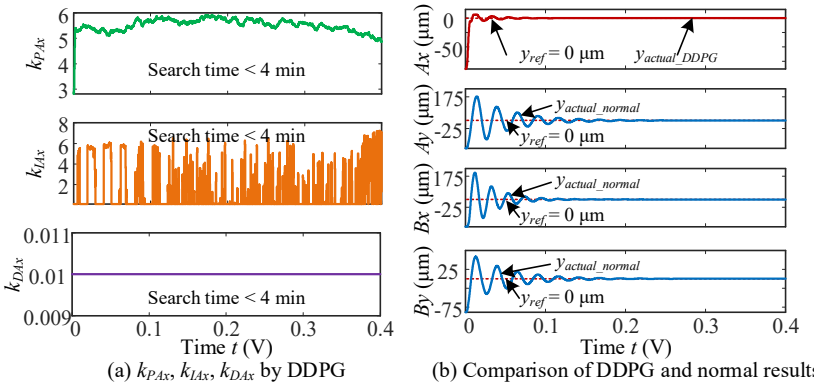

(a) k_{PAx}, k_{IAx}, k_{DAx} by DDPG (b) Comparison of DDPG and normal results

Fig. 5 Comparison of rotor floating displacement based on DDPG and conventional PID

Fig. 5(a) shows the final PID controller parameters for *Ax* self-tuned by DDPG, which took less than 4 minutes. Fig. 5(b) displays the levitation curves of the four DOFs, demonstrating that all four DOFs achieve stable levitation and verifying that the DDPG-based self-tuning method can turn AMBs from unstable to stable. Additionally, *Ax* shows smaller overshoot and settling time than other DOFs, proving stronger robustness of DDPG-based PID self-tuning method. Notably, DDPG-tuned PID parameters vary continuously, enabling adaptive adjustments via system feedback to minimize vibrations. This breaks from traditional fixed PID parameters, offering greater value for online self-tuning.

4.2 Results under sinusoidal disturbance

Rotors encounter various sinusoidal disturbance (unbalance, misalignment, or unbalanced magnetic pull) in practical applications, which manifests as single or superimposed sinusoidal excitation. Controllers must ensure strong robustness under such condition. The performance of anti-sinusoidal disturbance of DDPG-based method is conducted and analyzed.

Fig. 6(a) shows the final PID parameters for DOF *Ax* self-tuned by DDPG within 4 minutes. Fig. 6(b) presents levitation curves for all four DOFs. Under identical sinusoidal disturbances, the vibration amplitude of *Ax* is significantly smaller than *Ay*, *By*, and *By*, verifying superior robustness of the DDPG self-tuning method.

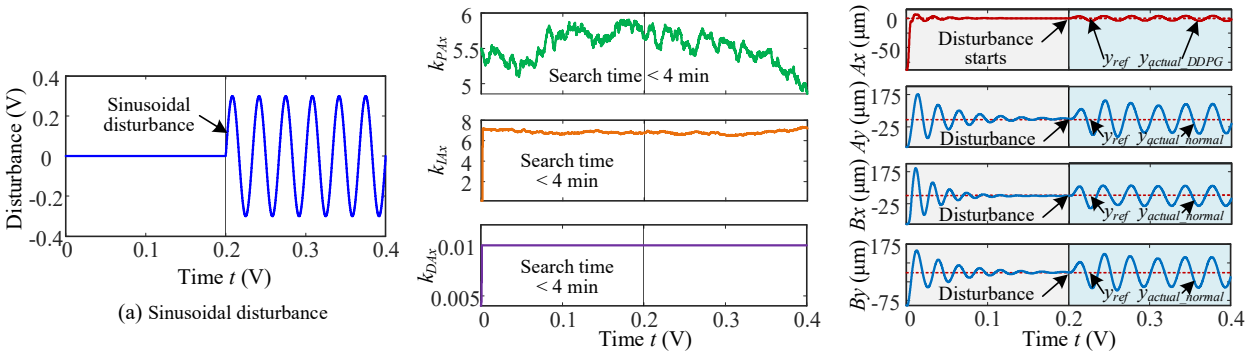

(a) Sinusoidal disturbance (b) k_{PAx}, k_{IAx}, k_{DAx} by DDPG (c) Comparison of DDPG and normal results

Fig. 6 Comparison of rotor displacement based on DDPG and conventional PID under sinusoidal disturbance

4.3 Results under step disturbance

To ensure the controller's robustness against step disturbance, the performance of anti-step disturbance of DDPG-based method is conducted. Fig. 7(a) shows the final PID parameters for DOF *Ax* self-tuned by DDPG within 4 minutes. Fig. 7(b) presents levitation curves for all four DOFs. Under identical step disturbance, the vibration amplitude of DOF *Ax* is significantly smaller than *Ay*, *By*, and *By*, confirming superior robustness of DDPG self-tuning method.

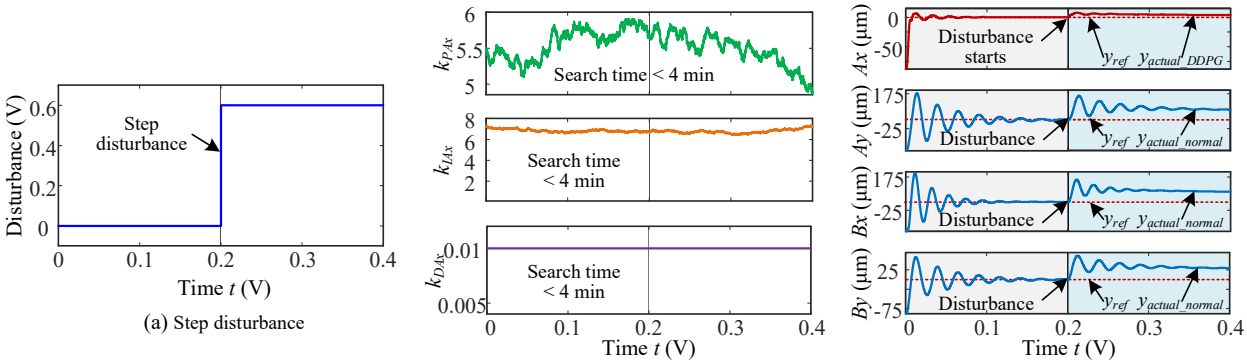

(a) Step disturbance (b) k_{PAx}, k_{IAx}, k_{DAx} by DDPG (c) Comparison of DDPG and normal results

Fig. 7 Comparison of rotor displacement based on DDPG and conventional PID under step disturbance

4.4 Results under shock disturbance

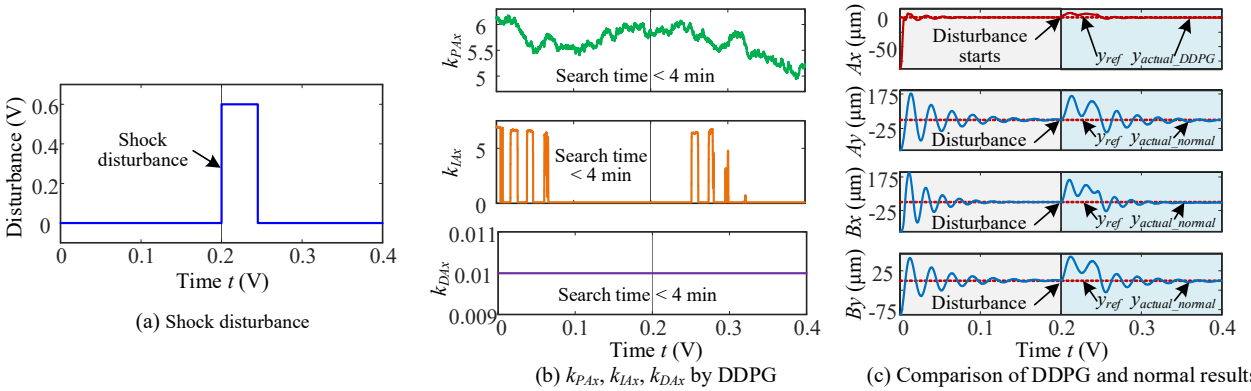

(a) Shock disturbance (b) k_{PAx}, k_{IAx}, k_{DAx} by DDPG (c) Comparison of DDPG and normal results

Fig. 8 Comparison of rotor displacement based on DDPG and conventional PID under shock disturbance

To ensure the controller's robustness against shock disturbance, the performance of anti-shock disturbance of DDPG-based method is conducted. Fig. 8(a) shows the final PID parameters for DOF *Ax* self-tuned by DDPG within 4 minutes. Fig. 8(b) presents levitation curves for all four DOFs. Under identical shock disturbance, the vibration amplitude of DOF *Ax* is significantly smaller than *Ay*, *By*, and *By*, confirming superior robustness of the DDPG self-tuning method.

4.5 Results under composite disturbance

Combined disturbances integrating the aforementioned sinusoidal, step, and impulse disturbances are more prevalent in practical industrial applications. A performance test of anti-composite disturbance of DDPG-based method is conducted. Fig. 9(a) shows the final PID parameters for DOF *Ax* self-tuned by DDPG within 5 minutes. Fig. 9(b) presents levitation curves for all four DOFs. Under identical composite disturbances, the vibration amplitude of DOF *Ax* is

significantly smaller than *Ay*, *By*, and *By*, confirming superior robustness of the DDPG self-tuning method.

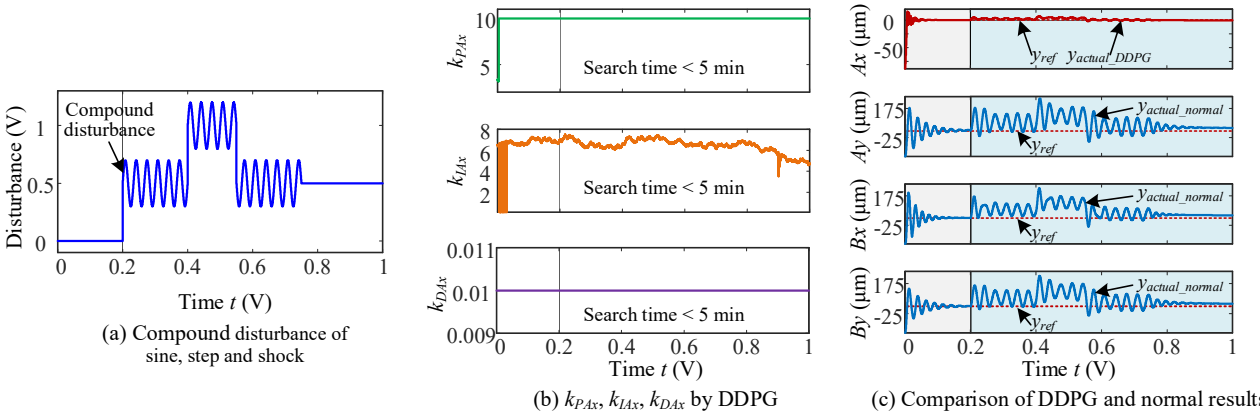

(a) Compound disturbance of sine, step and shock

(b) k_{PAx}, k_{IAx}, k_{DAx} by DDPG

(c) Comparison of DDPG and normal results

Fig. 9 Comparison of rotor displacement based on DDPG and conventional PID under composite disturbance

5. Conclusion

This paper addresses problem of PID controller parameter tuning in AMBs by proposing a DDPG-based self-tuning method. Conventional PID parameters are derived by establishing mathematical model of a closed-loop system. To solve the problem of PID parameters tuning, DDPG methodology and its underlying principles for AMB applications are elucidated, and an improved reward function enabling fast convergence across wide action spaces is designed and analyzed. Finally, comprehensive validation of DDPG self-tuning method under static levitation, sinusoidal, step, impulse, and composite disturbances are conducted. Results confirms that the DDPG-tuned PID controller not only self-tunes optimal levitation parameters but also achieves superior robustness.

Critically, the self-tuning method reduces the complexity of controller design for AMB engineers. The rapid wide-range convergence capability diminishes precise action-space calibration requirements across diverse applications (blowers, compressors, vacuum pumps), accelerating AMB standardization and industrial deployment.

6. Acknowledgments and conflicts of interest

This work was supported by the National Natural Science Foundation of China (52475060).

The authors declare that they have no known competing financial interests or personal relationships that could have appeared to influence the work reported in this paper.

References

Koehler, B. U., Denk, J., Van Maanen, et al., Applying standard industrial components for active magnetic bearings, Actuators, Vol.6, No.1 (2017), pp.8.

Yu, Q., Cao X., Deng X., et al., A Negative Stiffness Injection Method to Reduce Vibration for PMSM in 5-DoF Magnetic Levitation Systems, IEEE Transactions on Industrial Electronics (2025), pp.1-12.

Li, L., Xu, X., Li, J., et al., A low-power precise control of active magnetic bearing system based on dynamic LQR and Kalman filter, Electrical Engineering (2025), pp.1-9.

Zhang, Y., Xu, Y., Zhou, J., et al., Vibration Control of AMB-Rotor System Under Base Motions Based on Disturbance Observer, IEEE/ASME Transactions on Mechatronics (2025), pp.1-10.

Sarmah, N., Tiwari, R., Numerical and experimental study on quantitative assessment of multiple fault parameters in a warped internally damped rotor with a transverse fatigue crack integrated with an active magnetic bearing, Mechanical Systems and Signal Processing, Vol. 174 (2022), pp.109112.

Hutterer, M., Wimmer, D., Schrödl, M, Stabilization of a magnetically levitated rotor in the case of a defective radial actuator, IEEE/ASME Transactions on Mechatronics, Vol.25, No.6 (2020), pp.2599-2609.

Laldingliana, J., Biswas, P. K., Artificial intelligence based fractional order PID control strategy for active magnetic bearing, Journal of Electrical Engineering & Technology, Vol.17, No.6 (2022), pp.3389-3398.

Liu, X., Ma, X., Zheng, S., et al., Feedback linearization and robust control for whirl mode with operating point deviation in active magnetic bearings-rotor system, IEEE Transactions on Industrial Electronics, Vol.70, No.8 (2022), pp.7673-7682.

Mousavifard, R., Alipour, K., Najafqolian, M. A., et al., Quadrotor trajectory tracking using combined stochastic model-free position and DDPG-based attitude control, ISA transactions, Vol.156 (2025), pp.240-252.